



ELSEVIER

Contents lists available at ScienceDirect

Journal of Magnetism and Magnetic Materials

journal homepage: www.elsevier.com/locate/jmmm

Magnetic properties of nanoscaled paramelaconite $\text{Cu}_4\text{O}_{3-x}$ ($x=0.0$ and 0.5)

D. Djurek^{a,*}, M. Prester^b, Dj. Drobac^b, M. Ivanda^c, D. Vojta^c^a A. Volta Applied Ceramics (AVAC), 49247 Zlatar Bistrica, A. Šenoe 14, Croatia^b Institute of Physics, 10000 Zagreb, Bijenička c. 46, Croatia^c Ruđer Bošković Institute, 10000 Zagreb, Bijenička c. 54, Croatia

ARTICLE INFO

Article history:

Received 25 November 2013

Received in revised form

20 February 2014

Accepted 3 April 2014

Keywords:

Pyrochlore lattice

Superexchange

Superparamagnetism

Inversion symmetry

Dzyaloshinsky–Moriya interaction

ABSTRACT

Pure paramelaconite $\text{Cu}_4\text{O}_{3-x}$ has been prepared in the form of nanoparticles with 56 nm in diameter. This mixed valency oxide crystallizes in a tetragonal lattice with 4 unit formulae and forms a pyrochlore structure which manifests in two stoichiometric forms; Cu_4O_3 and $\text{Cu}_4\text{O}_{2.5}$, the latter form having two oxygen vacancies per unit cell. Magnetic lattice consists of Cu spin 1/2, and both stoichiometric forms obey transition to the antiferromagnetic state at $T_N=45\text{--}55$ K. Defect free Cu_4O_3 is indicated by an inversion symmetry and exhibits both antiferromagnetic and ferromagnetic state, where the latter is supposedly due to the superexchange interaction in Cu–O(1 π)–Cu bonds. An additional magnetic transition was observed in Cu_4O_3 at $T=120$ K, probably as a result of an incommensurate ordering. Absence of an inversion symmetry in the oxygen defect $\text{Cu}_4\text{O}_{2.5}$ results in a long range Dzyaloshinsky–Moriya interaction accompanied by the strong superparamagnetism.

© 2014 Published by Elsevier B.V.

1. Introduction

Intermediate copper oxide $\text{Cu}_4\text{O}_{3-x}$ coined paramelaconite, meaning a derivative of melaconite CuO (today tenorite) has been discovered [1,2] as a natural mineral sample in Arizona 1891 (Copper Queen Mine in Bisbee). The first examinations of the structure of the mineral sample were reported by Frondel [3], and subsequent studies [4,5] revealed the tetragonal unit cell containing 4 unit formulae $\text{Cu}_4\text{O}_{3-x}$ as shown in Fig. 1. Lattice parameters are: $a=583.7$, $c=993.20$ pm, and crystal symmetry is ditetragonal dipiramidal with H–M group $4/mmm$.

Paramelaconite is a mixed valency oxide $\text{Cu}_2^{2+} + \text{Cu}_2^+ \text{O}_3$, and Cu^{2+} cations form corner shared tetrahedrons with oxygen O(2) in the centre, characteristic for pyrochlore lattices which usually consist of four face-centred cubic sublattices. Tetrahedrons are extended along a - and b -axis, as presented in Fig. 2. It is noteworthy that two oxygen O(1) atoms per unit cell are positioned at $z=0.1162$, instead $z=1/8$ as it is in the case of O(2). In addition to Fig. 1 one may visualize the pyrochlore lattice in a way sketched by Enjalran and shown in inset of Fig. 3.

Corner shared tetrahedrons in pyrochlore lattices form face triangles, and structure is quoted as kagomé lattice. Interactions

among nearest neighbour spins J_{ij} are indicated by geometric frustration, meaning that one cannot simultaneously minimize the total energy of three spins in triangles. This results in an infinitely degenerate ground state at absolute zero.

However, magnetic properties of the paramelaconite investigated by Pinsard-Gaudart and co-workers [6] revealed very weak neutron diffractions indexed in the magnetic vector $k=(1/2,1/2,1/2)$, which may be attributed to a weak ferromagnetism. This means in turn that the ground state may not be indicated by infinite degeneracy characteristic for equilateral triangular kagomé lattices. In contrast, faces of Cu–O(2) tetrahedrons in paramelaconite form isosceles triangles, and frustration may be, at least, partial. Authors spotted antiferromagnetic transition at $T_N=42.3$ K, and paramelaconite is the first observed pyrochlore compound exhibiting a magnetic lattice with spin $S=1/2$. Neutron diffraction data motivated Elhajal and co-workers [7,8] to consider Dzyaloshinsky–Moriya interaction in the paramelaconite.

Mineral sample usually contains unwanted magnetic impurities coming from CuO which may considerably affect measurements. In this paper we present data recorded on laboratory prepared high purity paramelaconite, which obeys two stoichiometric modifications; Cu_4O_3 and $\text{Cu}_4\text{O}_{2.5}$. Both modifications are indicated by simultaneous appearance of the antiferromagnetic and ferromagnetic order, while the latter order may explain the neutron reflections indexed in the magnetic propagation vector $k=(1/2,1/2,1/2)$. Oxygen defect $\text{Cu}_4\text{O}_{2.5}$ is antiferromagnetic, with superimposed

* Corresponding author.

E-mail address: daniel.djurek@zg.t-com.hr (D. Djurek).

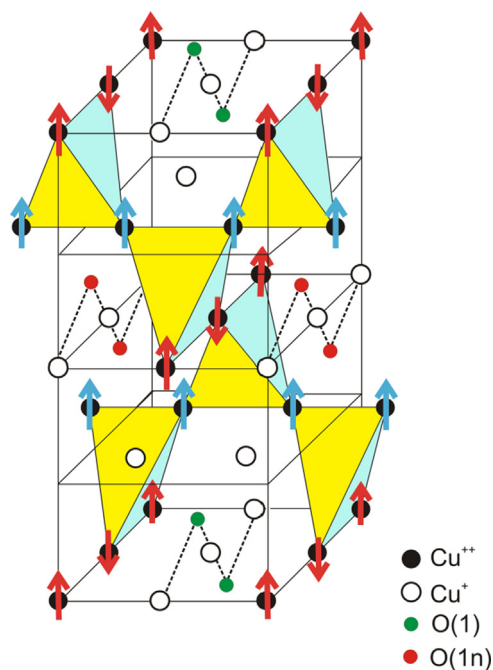


Fig. 1. Unit cell of paramelaconite Cu_4O_3 . Proposed magnetic cell is visualized by arrows showing possible antiferromagnetic and ferromagnetic $k=(1/2, 1/2, 1/2)$ order.

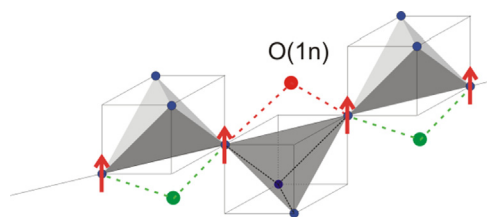


Fig. 2. Chain of Cu-O(2) tetrahedrons extended along a -axis. Blue and green dots represent Cu and O(1) atoms in Cu_4O_3 , respectively. Red dot represents oxygen atom O(1n) in the non-equivalent position, while in $\text{Cu}_4\text{O}_{2.5}$ this position means oxygen vacancy. Red arrows symbolize ferromagnetic Cu-O(1n)-Cu superexchange ordering. (For interpretation of the references to color in this figure legend, the reader is referred to the web version of this article.)

ferromagnetic order coming from the long range Dzyaloshinsky-Moriya interaction. Ferromagnetism in the nanoparticles of the paramelaconite gives rise to the strong superparamagnetism extending up to room temperature.

2. Experiment

Powders of paramelaconite were prepared by oxidation of Cu_2O or reduction of CuO , the latter method being performed in the mixture of hydrogen and argon. Cu_4O_3 is stable at temperatures 673–750 K, while oxygen defect $\text{Cu}_4\text{O}_{2.5}$ forms at 750–810 K.

Average particle size of the powder reported in this paper was 56 nm, and we denote paramelaconite also as $\text{Cu}_4\text{O}_{3-x}$ with $x=0$ and $x=0.5$.

Magnetic AC susceptibility measurements were performed by use of high resolution CryoBIND AC susceptibility system. Powders of Cu_4O_3 and $\text{Cu}_4\text{O}_{2.5}$ were prepared for AC susceptibility measurement in two ways; as weakly compacted form and cast in epoxy resin. Casting in epoxy resin was performed in PTFE die and specimens were 4 mm in diameter and 5 mm in length.

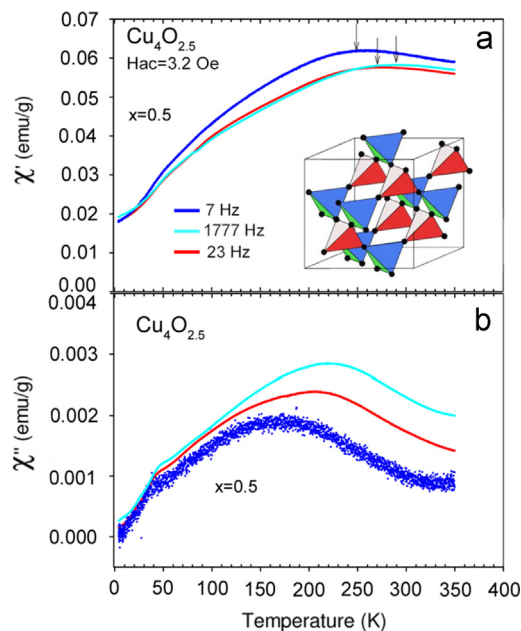


Fig. 3. AC susceptibility of the weakly compacted powder of $\text{Cu}_4\text{O}_{2.5}$; (a) real part and (b) imaginary part. Inset shows pyrochlore lattice visualized by Enjalran.

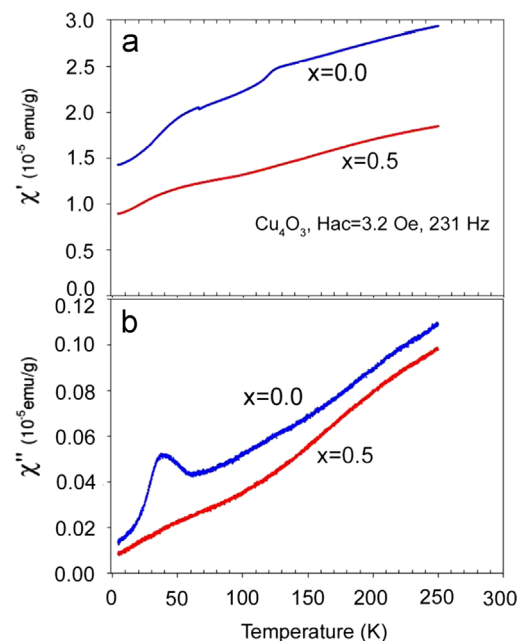


Fig. 4. AC susceptibility of Cu_4O_3 (blue) and $\text{Cu}_4\text{O}_{2.5}$ (red) powder cast in epoxy; (a) real parts, (b) imaginary parts. (For interpretation of the references to color in this figure legend, the reader is referred to the web version of this article.)

2.1. Oxygen defect $\text{Cu}_4\text{O}_{2.5}$

(a) AC susceptibility was measured on the weakly pressed powder and data are shown in Fig. 3a. It is evident strong contribution of the superparamagnetism in the temperature range 55–250 K. At $T < 55$ K antiferromagnetic transition takes place, in agreement with data presented in [6]. In the high-temperature superparamagnetic range AC susceptibility is frequency dependent, and temperature dependence of the imaginary part is shown in Fig. 3b. Fig. 4 shows the AC susceptibility of the powder $\text{Cu}_4\text{O}_{2.5}$ cast in epoxy resin; (a) real part of the susceptibility exhibits the change of the slope at 40–55 K, while no feature was observed in temperature dependent imaginary part (b).

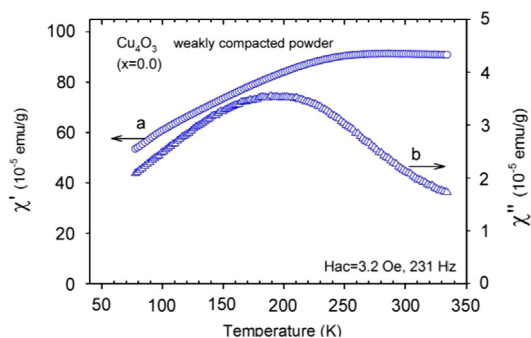


Fig. 5. AC susceptibility of a weakly compacted powder of Cu_4O_3 ; (a) real part and (b) imaginary part.

2.2. Defect free Cu_4O_3

Temperature dependence of AC susceptibility of the powder (~ 60 mg) of defect free Cu_4O_3 cast in epoxy resin is shown in Fig. 4. It is evident an apparent low value of the susceptibility as compared to that shown in Fig. 3 and reported in [6]. In order to remove possible spurious contributions from the sample holder necessary runs were undertaken without sample. In addition to cited antiferromagnetic transition at $T=45\text{--}55$ K another transition was observed at $T=120$ K, as it is visible in Fig. 4a. Superparamagnetic contribution is weak, and imaginary part of the susceptibility (Fig. 4b) exhibits a strong dissipation-related peak. It is important to note an absence of any feature at 200–230 K usually coming from the unwanted magnetic contributions in CuO.

Temperature dependence of AC susceptibility measured in a weakly compacted powder Cu_4O_3 is shown in Fig. 5, and it is visible from the real part (a) superparamagnetic contribution sounding for ferromagnetic long range interactions. A comparatively strong dissipation peak, attributed to the Néel relaxation of the grain magnetization, was traced in imaginary part (b).

3. Discussion

It was shown that nanoscaled paramelaconite $\text{Cu}_4\text{O}_{3-x}$ appears in two stoichiometric forms, which enables the separate study of magnetic effects in distorted ($x=0.5$) and undistorted ($x=0$) lattice. We suppose that in distorted unit cell two oxygen atoms $\text{O}(1n)$ in neighbourhood of two tetrahedrons are missed. Such an assumption may be extended to the mineral sample and we are led to believe that distortion in the mineral sample may come from the oxygen vacancies. Further supports in favour of defect natural sample are provided by density data [5] giving density 2.7% smaller than crystallographic density (5.89 g cm^{-3}). This should be compared to 2.5% of density contributed from two oxygen atoms per unit cell. In addition, chemical analysis performed by Frondel [3] gives $\text{Cu}_{16}\text{O}_{14}$, which suggests that mineral sample is mixture of CuO in molar fraction near 20% plus fraction having oxygen defect unit cell formula $\text{Cu}_{16}\text{O}_{10}$. This assumption is further supported by a comparatively strong contribution of CuO to the susceptibility visible at $T=230$ K, as reported in [6].

Data recorded by Raman (Fig. 6) and FTIR spectroscopy (Fig. 7) demonstrate an absence of inversion symmetry in oxygen defect $\text{Cu}_4\text{O}_{2.5}$ and an evidence of such symmetry in defect free Cu_4O_3 , the latter being indicated by the absence of the Raman modes originally traced in $\text{Cu}_4\text{O}_{2.5}$. The inversion symmetry allows the infrared modes, while it forbids the Raman modes and vice-versa.

Pyrochlore lattices are indicated by superexchange interactions, and qualitative understanding of such interactions poses a serious problem, notably in paramelaconite which is indicated by the

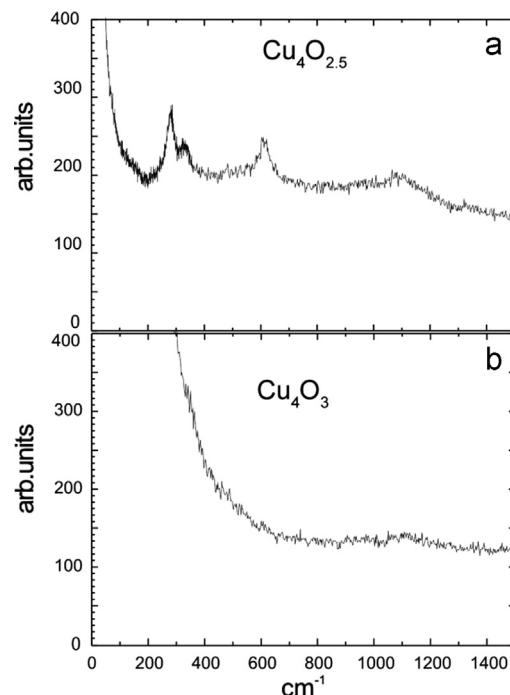


Fig. 6. Raman spectra of $\text{Cu}_4\text{O}_{2.5}$ (a) and Cu_4O_3 (b).

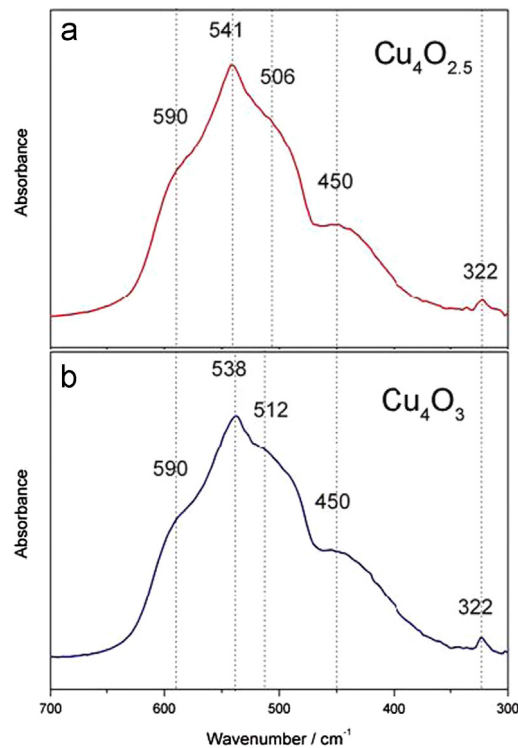


Fig. 7. FTIR spectra of $\text{Cu}_4\text{O}_{2.5}$ (a) and Cu_4O_3 (b).

strong electron localization present in a Mott-Hubbard insulator [9,10]. Localized electrons, however, may not serve as starting terms in calculation of interactions among them since localization itself is caused by their mutual interactions.

3.1. Antiferromagnetic interaction

Crystallographic and neutron scattering data suggest that the pyrochlore lattice Cu_4O_3 may not undergo geometrical frustration

of the spin 1/2 system. Presence of the partial ferromagnetic order requires a separate consideration of the ground state, and the antiferromagnetic subsystem may obey only finite degeneracy without long range order. However, quantum fluctuations [11] over antiferromagnetic magnon gap in the nanoparticle may lift any degeneracy by creation of an effective magnetic field H_{eff} . We consider here quantum fluctuations over gap E_0 coming from the zero point excitation of optical magnons in antiferromagnetic sublattices, and H_{eff} reduces nominal ground state field given by $H_{gs} = 2S\mu_B N/V$. Unit cell volume of Cu_4O_3 is $3.38 \times 10^{-28} \text{ m}^3$ giving $H_{gs} \sim 2.2 \times 10^5 \text{ A m}^{-1}$. Calculation of H_{eff} is not a straightforward task and has been performed for some special low dimensional cases [12]. Antiferromagnetic magnons, however, obey dispersion relation similar to that of photons, meaning that energy is linearly dependent on the wave number. This makes possible to consider excitations in nanoscaled particles of volume V_0 in the same way as a vacuum photon excitations in an optical resonant microcavity developed by Haroche [13]. Excitation field in the nanoparticle of volume V_0 over gap E_0 may then be given as $H_{eff} = (2E_0/\mu V_0)^{1/2}$. In order to remove divergence for very small volumes, such an approach deserves more detailed analysis of magnetic nanoparticles. Model proposed by Skomski [14] introduces a nanomagnetic length scale [15] and is described by differential equation

$$\Delta\varphi - \kappa^2\varphi = f(r) \quad (1)$$

which is modified Poisson equation with interaction length $1/\kappa$. Above expression for H_{eff} may be valid for nanoparticle diameter extended down to Skomski scale $2\pi/\kappa - a_0/\alpha$, where a_0 is magnetic lattice spacing, and $\alpha = 4\pi e_0 e^2/\hbar c = 1/137$ is fine-structure constant. Interaction length was evaluated to be $1/\kappa \sim 7.52 \text{ nm}$. An exact value of the energy gap in Cu_4O_3 is not known, and we use $E_0 = 2.2 \times 10^{-23} \text{ J}$ reported for antiferromagnet $\text{Ca}_3\text{Fe}_2\text{Ge}_3\text{O}_{12}$ [16] as a trial value. Calculation then gives for nanoparticles of Cu_4O_3 used in this work $H_{eff} \sim 1.5 \times 10^4 \text{ A m}^{-1}$, and $H_{eff}/H_{gs} \sim 0.07$, while for Skomski scale $H_{eff} - H_{gs}$, which seems to be a reasonable result. Skomski diameter $1/\kappa$ may appear in this case as a lower volume cut-off for application of above microcavity expression. Calculated H_{eff} will act as an external field and tend prefer a particular ordered ground state. In contrast of the infinite degeneracy in bulk samples, effective field in nanoparticle lifts degeneracy, and accompanying order may be understood as being driven by the fluctuation disorder.

Similarly as in the case of the optical resonant microcavities the strongest amplitudes have magnons with wavelengths comparable to the nanoparticle diameter, and these magnons couple to phonons giving rise to the apparent dissipation indicated by the imaginary part of the magnetic susceptibility shown in Fig. 4.

Appearance of an additional magnetic transition in Cu_4O_3 at $T = 120 \text{ K}$ is not understood so far. However, in some other pyrochlore lattices like CuFeO_3 [17] two successive antiferromagnetic transitions appear at $T = 14$ and 11 K as a result of incommensurate and commensurate magnetic order.

3.2. Ferromagnetic interaction

Appearance of the superparamagnetism in the weakly compacted powder of defect free Cu_4O_3 (Fig. 5) sounds for a ferromagnetic contribution and superimposed to antiferromagnetic interaction. Absence of an inversion symmetry excludes the possible ferromagnetism associated with Dzyaloshinsky–Moriya interaction in Cu_4O_3 , while weak ferromagnetism may be understood by superexchange interactions in Cu–O(1n)–Cu bonds indicated by an angle 94.5° .

According to third Goodenough–Kanamori–Anderson (GKA) rule [18–20] a weak ferromagnetic exchange may appear in 90° bond when orbitals are filled, as it is shown in Fig. 8. Oxygen p_z orbital couples with Cu- d_z^2 orbital, while oxygen p_y orbital couples with other Cu- d_z^2 orbital. In a virtual intermediate state two holes

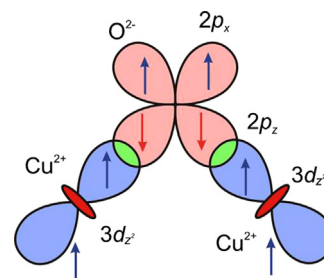


Fig. 8. Ferromagnetic superexchange interaction due to the first Hund's rule in Cu–O(1n)–Cu bond of Cu_4O_3 .

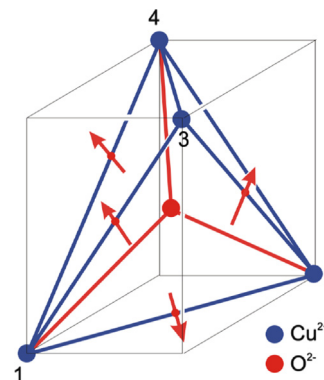


Fig. 9. Cu–O(2) tetrahedron. Red arrows represent Dzyaloshinsky–Moriya vectors \mathbf{D}_{ij} . Note that each vector attached to the particular edge is parallel to the opposite edge. Two vectors are omitted for clarity. (For interpretation of the references to color in this figure legend, the reader is referred to the web version of this article.)

appear on oxygen place and there are two possible states for two spins which in turn couple with Cu spins giving rise to the parallel orientation in agreement with the first Hund's rule.

Possible ferromagnetic order in the unit cell is visualized by arrows in Fig. 1, and this order may explain appearance of the propagation vector $k = (1/2, 1/2, 1/2)$ reported in neutron scattering measurements [6](Fig. 9).

3.3. Dzyaloshinsky–Moriya interaction

Dzyaloshinsky [21] and Moriya [22] involved relativistic contribution of spin–orbit coupling in the interaction Hamiltonian and postulated *anisotropic* superexchange interaction. Isotropic part of the superexchange interaction in the tetrahedron presented in Fig. 8 deals with two contributions; $J_1 = J_{12} = J_{34}$, $J_2 = J_{14} = J_{24} = J_{23}$, and Hamiltonian turns out to be

$$H = \sum_{ij} J_{ij} S_i S_j + \sum_{ij} \mathbf{D}_{ij} (S_i \times S_j) \quad (2)$$

According to the first Moriya's rule \mathbf{D}_{ij} is nonzero only if inversion centre of tetrahedron in Fig. 8 is not located at the oxygen atom. Cross product is finite due to the *chirality* [23], and data evaluated from the Raman and FTIR suggest that these rules are satisfied in $\text{Cu}_4\text{O}_{2.5}$. \mathbf{D}_{ij} vectors may be evaluated by use of the second order perturbation procedure [24] considering two contributions in the Hamiltonian of the localized electron.

$$H = H_0 + H_1 \quad (3)$$

$$H_0 = p^2/2m + e \times V(r) \quad (4)$$

$$H_1 = (e \times \hbar/2m^2 c^2) S [\nabla V(r) \times p] \quad (5)$$

DMI contribution is governed by third relativistic term expressing spin–orbit coupling, and electron feels the gradient of the crystal field $V(r)$. This contribution may be quite important in

oxygen defect $\text{Cu}_4\text{O}_{2.5}$. Two tetrahedrons in the unit cell are accompanied by two oxygen vacancies as it may be recognized from Fig. 2.

Similarly as in Cu–O tetrahedrons positioned in Cu_2O unit cell [23], oxygen vacancies may induce strong gradients of the crystal field on electron sites. AC susceptibility measured in a weakly compacted powder of $\text{Cu}_4\text{O}_{2.5}$ is nearly two orders of magnitude higher than that in corresponding powder of Cu_4O_3 . This difference may be attributed to the long range order formed by the competition between ferromagnetic exchange interaction and DMI [25].

4. Conclusion

Nanoscaled intermediate copper oxides $\text{Cu}_4\text{O}_{3-x}$ (paramelaconite) have been prepared in laboratory and arguments were presented in favour of two possible stoichiometric modifications. Cu_4O_3 is indicated by undistorted tetragonal lattice, while the other stoichiometric modification forms the tetragonal lattice with two oxygen vacancies giving unit formula $\text{Cu}_4\text{O}_{2.5}$. The undistorted modification is further indicated by an inversion symmetry and exhibits a weak ferromagnetism, as well as an antiferromagnetic ordering at $T < 55$ K. $\text{Cu}_4\text{O}_{2.5}$ is indicated by distortion of copper tetrahedrons in the vicinity of oxygen vacancies and formation of both antiferromagnetic and Dzyaloshinsky–Moriya interaction. At $T > 55$ K the superparamagnetic state persists in both stoichiometric forms and it extends up to room temperature.

It was observed an additional magnetic transition at $T = 120$ K in defect free paramelaconite Cu_4O_3 , which needs more clarification in the future work.

Acknowledgment

Authors are indebted to Dr Enjalran for permission to reproduce pyrochlore lattice drawing in Fig. 3.

References

- [1] G.A. Koenig, Proc. Acad. Nat. Sci. Phil. (1891) 284.
- [2] S.A. Williams, Am. Mineral. 47 (1962) 778.
- [3] C. Frondel, Am. Mineral. 26 (1941) 657.
- [4] M. O'Keeffe, S. Andersson, Acta Crystallogr., Sect. A: Found. Crystallogr. 33 (1977) 914.
- [5] M. O'Keeffe, J.O. Bovin, Am. Mineral. 63 (1978) 180.
- [6] L. Pinsard-Gaudart, J. Rodriguez-Carvajal, A. Gukasov, P. Monod, Phys. Rev. B: Condens. Matter 69 (2004) 104408.
- [7] M. Elhajal, B. Canals, C. Lacroix, J. Phys. Condens. Matter 16 (2004) S917.
- [8] M. Elhajal, B. Canals, R. Sunyer, C. Lacroix, Phys. Rev. B: Condens. Matter 71 (2005) 094420.
- [9] N.F. Mott, Proc. Phys. Soc. London, Sect. A 62 (7) (1949) 416.
- [10] J. Hubbard, Proc. Phys. Soc. London 276 (1365) (1963) 238.
- [11] T. Yildirim, Turk. J. Phys. 23 (1999) 47.
- [12] T. Ishikawa, T. Oguchi, Prog. Theor. Phys. 54 (1975) 1282.
- [13] S. Haroche, D. Kleppner, Phys. Today 42 (1989) 24.
- [14] R. Skomski, Simple Models of Magnetism, Oxford University Press Inc., New York (2008) 2008270.
- [15] R. Skomski, J. Magn. Magn. Mater. 272-276 (2004) 1476.
- [16] A.G. Gukasov, Th. Brückel, B. Dorner, V.P. Plakhty, W. Prandl, E.F. Shender, O.P. Smirnov, Europhys. Lett. 7 (1) (1988) 83.
- [17] F. Ye, Y. Ren, Q. Huang, J.A. Fernandez-Baca, Pengcheng Dai, J.W. Lynn, T. Kimura, Phys. Rev. B: Condens. Matter 73 (2006) 220404.
- [18] J.B. Goodenough, J. Phys. Chem. Solids 6 (1958) 287.
- [19] J. Kanamori, Prog. Theor. Phys. 17 (1957) 177.
- [20] P.W. Anderson, Phys. Rev. 79 (1950) 350.
- [21] I. Dzyaloshinsky, J. Phys. Chem. Solids 4 (1958) 241.
- [22] T. Moriya, Phys. Rev. 120 (1960) 91.
- [23] H.-J. Mikeska, A.K. Kolezhuk, Lect. Notes Phys. 645 (2004) 1.
- [24] F. Biccari, Thesis SAPIENZA (2009).
- [25] H.Y. Kwon, K.M. Bu, Y.Z. Wu, C. Won, J. Magn. Magn. Mater. 324 (2012) 2171.